Mutations of an Epitope Hot-Spot Residue Alter Rate Limiting Steps of Antigen−Antibody Protein−Protein Associations

Yili Li,[‡] Claudia A. Lipschultz, S. Mohan,[§] and Sandra J. Smith-Gill*

Basic Research Laboratory, Program in Structural Biology, National Cancer Institute, Frederick Cancer Research and Development Center, P.O. Box B, Building 469, Room 206, Frederick, Maryland 21702-1201 USA

Received June 20, 2000; Revised Manuscript Received October 3, 2000

ABSTRACT: The antibodies, HyHEL-10 and HyHEL-26 (H10 and H26, respectively), share over 90% sequence homology and recognize with high affinity the same epitope on hen egg white lysozyme (HEL) but differ in degree of cross-reactivity with mutant lysozymes. The binding kinetics, as measured by BIAcore surface plasmon resonance, of monovalent Fab from both Abs (Fab10 and Fab26) to HEL and mutant lysozymes are best described by a two-step association model consistent with an encounter followed by docking that may include conformational changes. In their complexes with HEL, both Abs make the transition to the docked phase rapidly. For H10, the encounter step is rate limiting, whereas docking is also partially rate limiting for H26. The forward rate constants of H10 are higher than those of H26. The docking equilibrium as well as the overall equilibrium constant are also higher for H10 than for H26. Most of the free energy change of association ($\Delta G°$) occurs during the encounter phase ($\Delta G1$) of both Abs. H10 derives a greater amount and proportion of free energy change from the docking phase ($\Delta G2$) than does H26. In the H10−HEL(R21Q) complex, a significant slowing of docking results in lowered affinity, a loss of most of $\Delta G2$, and apparently faster dissociation. Slower encounter and docking cause lowered affinity and a loss of free energy change primarily in the encounter step ($\Delta G1$) of H26 with mutant HEL(R21Q). Overall, in the process of complex formation with lysozyme, the mutations HEL-(R21X) affect primarily the docking phase of H10 association and both phases of H26. Our results are consistent with the interpretation that the free energy barriers to conformational rearrangement are highest in H26, especially with mutant antigen.

It is generally assumed that protein−protein associations involve at least two steps: an initial encounter or collision to form an intermediate encounter complex, followed by a docking or annealing that may involve conformational rearrangements of either or both components (*2*). Most structural studies have indicated these complexes conform largely to a "lock and key" type of mechanism, with significant small, concerted changes in the contact interface (*3*−*8*), and it has been suggested that affinity maturation of antibodies may involve stabilization of a favorable binding conformation (*9*, *10*). Recently, a set of catalytic antibodies have been shown by fluorescent quenching to undergo a rapid bimolecular association followed by one or two steps of unimolecular isomerization (*11*), even though previous X-ray studies had not indicated that conformational rearrangements accompanied binding. In these complexes, the isomerization led to tighter binding affinity and higher catalytic activity. This dynamic pattern of a rapid encounter followed by a relatively slow (t_2 3−5 min) rearrangement or docking has not previously been reported for noncatalytic antibodies specific for protein antigens, and the role of such a mechanism in specificity and affinity in the normal immune response remains to be defined.

Recently, we have shown that the association kinetics of the antibodies H26[1] and H10 conform well to a two-step binding model. H26 and H10 share over 90% sequence homology, and they are specific for highly coincident[2] epitopes on hen egg white lysozyme (HEL) but have different degrees of cross-reactivity with mutant antigens (*12*−*15*). H26 is more specific and more sensitive to mutations in the epitope than is H10. The differences in overall sensitivities

* To whom correspondence should be sent: P.O. Box B, Bldg 469, Room 206, NCI−FCRDC, Frederick, MD 21702-1201 USA. Phone: 301-846-5203. FAX: 301-846-6326. E-mail: smithgil@helix.nih.gov.

[‡] Current Address: Center for Advanced Research in Biotechnology, University of Maryland Biotechnology Institute, Rockville, MD 20850 USA.

[§] Current Address: Department of Chemical Engineering, University of Houston, Houston, TX 77204 USA.

[1] Abbreviations: H10, HyHEL-10; H26, HyHEL-26; Fab10 and Fab26, Fab portion of HyHEL-10 and HyHEL-26, respectively; rFab, recombinant Fab; rfFab, recombinant Fab expressed as separate H and L chains in inclusion bodies and refolded; chFab, chemical Fab produced by proteolytic digestion of native IgG; CDR, complementarity determining region; HEL, hen egg white lysozyme from the chicken; HEL(R21X), generic designation of HEL with mutations of residue $R21_{HEL}$; JQL, Japanese quail egg white lysozyme; Ab, antibody; Ag, antigen; H,L, heavy-light chains of IgG (or variable regions); rds, rate determining step; SPR, surface plasmon resonance.

[2] We use the term "coincident" to describe epitopes that are highly overlapping and have been found to be essentially identical both by epitope mapping techniques and in low resolution X-ray crystallography but likely have some different intermolecular contacts that might be revealed in high resolution X-ray structures. In agreement with this interpretation, a fourth antibody H63 whose epitope is also coincident with that of H10 by functional mapping has recently been shown by X-ray crystallography to recognize an epitope with nearly identical contacting residues as H10 (*1*).

10.1021/bi0014148 CCC: $20.00
Published on Web 01/25/2001

of the Abs to mutation in the antigen epitope reflect differences in the relative sensitivities of their association and dissociation rates (*14*). Complexes of H10 with mutant antigen show only small variations in their apparent on rates but large increases in their apparent off rates. In contrast, complexes of H26 with mutant antigens have significantly lower on rates as well as higher off rates (*16*).

The high affinity complexes of Fab10 and Fv10 with HEL have been structurally defined by X-ray crystallography (*17, 18*). In the Fab10−HEL complex, the amino acid residue $R21_{HEL}$ makes five contacts and two hydrogen bonds with the antibody, including contacts with five aromatic residues. Thermodynamic calculations and alanine scanning experiments indicate it is a major contributor to the free energy of association (*14, 19*−*22*), contributing ∼1.5−2 kcal/mol to ΔG of association. Most of the free energy loss in site-directed or natural species variants with substitutions at $R21_{HEL}$ occurred in the dissociation phase rather than in the association phase of binding ($\Delta\Delta G_{off} \geq 1$ kcal/mol > $\Delta\Delta G_{on}$) (*23*), while in H26 complexes with $R21_{HEL}$ variants the free energy loss occurs in both phases (*14*). The kinetics reported to date were observed in binding experiments of relatively short durations. Recently, we have shown (*24*) that for association times longer than 3−5 min, the binding kinetics of these mAbs is best described by a two-step bimolecular association model, consistent with a two-phase binding sequence of encounter followed by docking that may include conformational changes (*25*−*27*). Analysis by a two-step model is biologically appropriate to the system because computation analysis of H26 and H10 suggest differences between the antibodies in conformational flexibility. (Mohan, Sinha, and Smith-Gill, unpublished data). We utilize the two-step association model here to analyze the dynamics by which antigenic mutations of $R21_{HEL}$ lower the affinity of the H10 and H26 complexes. Our results are consistent with the interpretation that the free energy barriers to conformational rearrangement are highest in H26, especially with mutant antigen. Our results also suggest docking of H10 is particularly sensitive to mutations of $R21_{HEL}$, as the mutations primarily slow the docking step with only minor effects of the encounter phase. In H26 complexes, the initial encounter, as well as docking, is sensitive to mutations at $R21_{HEL}$. Our results are consistent with the hypothesis that H26 conforms more to the "lock and key" type of binding, deriving very little free energy change from the docking step.

EXPERIMENTAL PROCEDURES

Cloning of Antibody Genes and Construction of Expression Vectors. cDNA clones of the genes encoding the κ light chains and the IgG heavy chains of the two mAb, H10 and H26 (*15*) were isolated from the corresponding hybridoma cell mRNA. Reverse transcription (Promega, Madison, WI) yielded cDNA containing the light chain and the Fd-fragment of heavy chain genes of the antibodies which were then PCR amplified and ligated into pET-22b(+) (Novagen, Madison, WI) for secretory expression in electoporation transformants of *Escherichia coli* strain BL21(DE3). The cells were harvested by centrifugation, and the supernatant was stored at 4 °C until use. Concentration of Fab in supernatants were determined by immunoassay (*28*). Fabs were also produced by in vitro refolding (rfFabs) from H and L chain soluble fragments or isolated from 0.4 M L-arginine. The diluted solutions were kept at 4 °C for at least 96 h. rFabs were purified from *E. coli* supernatant or the refolding solution by direct application to an HEL affinity column, followed by FPLC on a Superdex200 column (Pharmacia). Fab10 was also produced by papain digestion of purified native H10 Ig and purification on Protein A and DEAE chromatography as described previously (*14*). Concentration of purified Fab fragments was determined directly using an extinction coefficient at 280 nm of 1.73 or by immunoassay (*29*), using purified Fab10 as a standard.

Surface Plasmon Resonance (SPR). HEL, site-directed mutants HEL(R21X), and JQL were immobilized to CM-5 sensor chips in a BIAcore1000 Biosensor (Biacore, Inc., Uppsala, Sweden) as described previously (*24*). Reduced half antibodies of H10 produced from purified native IgG, using 2-mercaptoethanolamine-HCL (MEA) to cleave the disulfides between the heavy chains (product instructions from Pierce Chemical Company, IL), were thiol coupled to the CM-5 sensor chip using the BIA handbook protocol for ligand-thiol immobilization. Binding of analyte (recombinant Fabs or JQL) was measured by surface plasmon resonance (SPR) in a BIAcore1000 or BIAcore 2000 in HBS buffer at 25 °C with association times ranging from 2 to 250 min and dissociation times ranging from 10 to 45 min. All chips included a control surface that consisted of trace amounts of HEL immobilized using the same chemistry as the experimental surfaces. The sensogram profile of each analyte sample on the control surface was subtracted from the corresponding experimental curves. Experiments utilizing varying surface densities of ligand and varying flow rates indicated that these variables did not significantly affect the binding parameters.

Estimates of Rate and Equilibrium Constants. We have shown previously (*24*) that the binding kinetics of H10 and H26 for association times longer than 3−5 min are best described by a two-step bimolecular association model corresponding to an "induced fit" binding mode:

$$A + B \underset{k_{-1}}{\overset{k_{+1}}{\rightleftharpoons}} [AB]^* \underset{k_{-2}}{\overset{k_{+2}}{\rightleftharpoons}} AB \qquad (1)$$

where A and B represent antibody and antigen, and [AB]* and AB represent encounter complex/transition state and docked/rearranged complexes, respectively (Figure 1). All complexes were evaluated initially from four to six binding curves with a flow rate of 10 μL/min and T_a of 10 and 25 min followed by a 25 min dissociation phase (*24*). Preliminary estimates of the rate parameters k_{+1}, k_{-1}, k_{+2}, k_{-2}, and R_{max} were made by global curve-fitting of these curves (simultaneous reiterative fits of all binding curves within a given data set) with BIAeval 3.0.2 software (Biacore, Inc., Uppsala, Sweden), and then the component curves for [AB]* and AB were simulated. We define the point at which these curves cross as T_{50}, where [AB]* = AB = 50%(RU_{total}) (Figure 1) (*24*). We have shown previously that reliable comparisons of goodness-of-fit, as well as estimates of the four rate constants for two-step kinetics, can be obtained only with data sets including variable association times (T_a) and that the most reliable estimates of the rate constants require a global analysis of data sets each containing T_a of at least two different durations, ideally at least one time shorter than

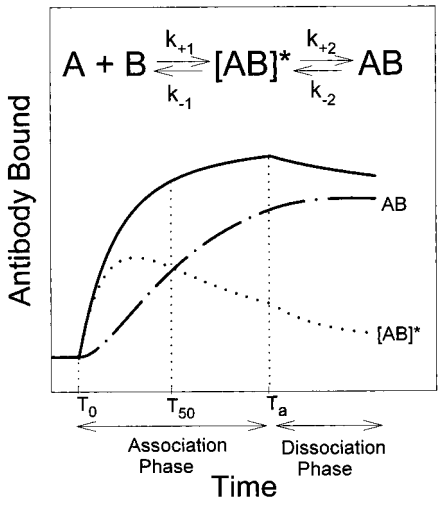

FIGURE 1: Diagram of sensogram with two-step components. Total response represents observed total RUs bound to which the model is fitted giving estimates of the four rate constants, k_{+1}, k_{-1}, k_{+2}, and k_{-2}; the component curves for the encounter complex [AB]* and docked complex AB are simulated from the experimentally determined rate constants.

the components crossover point ($T_a < T_{50}$) and one time greater than the components crossover point ($T_a > T_{50}$) (Figure 1) (*24*). Association profiles were therefore obtained for Fab10 and Fab26 with T_a ranging from 2−250 min. (Figure 2, panels a and b, and Figure 3, panels a and b). Using the rate constants determined above (Table 1), a series of simulations were performed for each of the wild type and mutant complexes to empirically determine comparable T_{50} for each complex (*24*). Equilibrium constants were calculated from the mean rate constants (Table 1) (*25*, *26*, *30*) Free energy changes accompanying the two association steps were calculated from the respective equilibrium constants:

$$\Delta G1 = -RT\ln(K\mathrm{a}_1) \text{ and } \Delta G2 = -RT\ln(K\mathrm{a}_2) \quad (2)$$

$$\Delta G^\circ = \Delta G1 + \Delta G2 = -RT\ln(K_\mathrm{A})$$

RESULTS

Analysis of Two-Step Kinetics. (a) Goodness-of-Fit, One-Step vs Two-Step Kinetic Models. Binding of these mAbs to mutant antigens frequently proceeds very slowly, requiring prolonged periods of association to obtain reliable estimates of kinetic parameters (*24*). All data sets incorporating variable T_a showed significantly better fits to the two-step model, both by statistical analysis and by inspection of the binding curves. The significant improvements in fit by the two-state model were manifest in both the association and dissociation phases of binding (Figure 2, panels a and b, and Figure 3, panels a and b).

(*b*) *Controls for Other Factors that Could Cause Apparent Complex Kinetics.* Other factors or artifacts could cause similar complex kinetics (*16*). Because it is not possible to distinguish among one-step vs multiple-step models by curve-fitting alone (*27*, *31*, *32*), we performed additional controls and experiments over those reported previously (*24*) to examine each of these possibilities. Detailed comparisons of binding curves established functional equivalence of rFab in unfractionated supernatant, rFab purified to homogeneity from *E. coli* supernatant, purified rfFab, and chFab (data shown in Supporting Information). Therefore, the two-step kinetics are not attributable to heterogeneity of analyte, and components in the unfractionated supernatant do not alter the binding kinetics of these antibodies. Purified rFab26 mixed with varying proportions of H26 IgG also showed that up to 30% whole IgG could be present without significantly changing the pattern of kinetics, indicating that if small amounts of dimeric or aggregated Fab had been undetected in our preparations they would not have caused the observed complex kinetics. Simulation experiments of mixtures of Fab and dimeric Fab (using rate consants determined from whole IgG) gave the same results. The affinity and stoichometry of gel filtration purified rfFab26 were also checked by analytical ultracentrifugation that showed it to be pure monomer with no indication of dimerization or aggregation during 3 days of centrifugation (P. Schultz, personal communication). These results support the conclusion that the observed two-step kinetics of the recombinant Fabs were not due either to heterogeneity of the Fab preps or caused by other factors in the *E. coli* supernatant.

(*c*) *Binding of Lysozyme to Antibody as Ligand Gives Two-Step Kinetics.* HyHEL-10 half antibody was thiol-coupled to the matrix and purified native JQL used as analyte. The resulting binding kinetics fit a two-step model (but not other complex models) significantly better than one-step (Figure 4). Therefore, the two-step process is not attributable to the heterogeneity of Fab preparations or nonspecific interactions such as interactions of Fab with the matrix.

(*d*) *Observed Off Rate Is a Time-Dependent Parameter*. We have shown previously that the net off rates of these complexes correlate inversely with the duration of the association phase (T_a; see Figure 1) (*24*). This is an expected result if the interaction between the receptor and the ligand reflects a multistep association involving an initial encounter followed by a slower docking to a more stable complex, because longer T_a's allow a higher proportion of stable AB (with a lower off rate) to form (*24*, *32*). The initial observed dissociation rate decreases by as much as 10-fold between the shortest (2 min) and longest (250 min). The relationship between T_a and k_{off} is a negative exponential relationship that is quantitatively unique for each Ab−Ag complex:

$$k_{off} = \mathrm{c}T_a^{-b} \quad (3)$$

The values of the exponential coefficient, *b*, for H10 complexed with either HEL ($b < 10^{-3}$) or HEL(R21Q) ($b = 0.16$) are less than the values of *b* for H26 complexed with either HEL ($b = 0.08$) or HEL(R21Q) ($b = 0.47$), respectively. For both Abs, the effect of the mutation is to increase the value of *b*, indicating a stronger dependence of the net off rate on time. Similar results have been observed for both Abs, as well as other functionally and structurally related Abs, on a variety of site-directed mutants of HEL (*24*).

(*e*) *The Complexes Reach Equilibrium Very Slowly.* We have observed previously that times of 18 h or more were necesssary for these antibodies to come to equilibrium in competitive binding ELISA or fluorescent immunoassays (*33*). It was also apparent that many of the complexes did not come to equilibrium in BIAcore binding experiments, even with T_a as long as 4 h (e.g., Figures 2b and 3b). It was

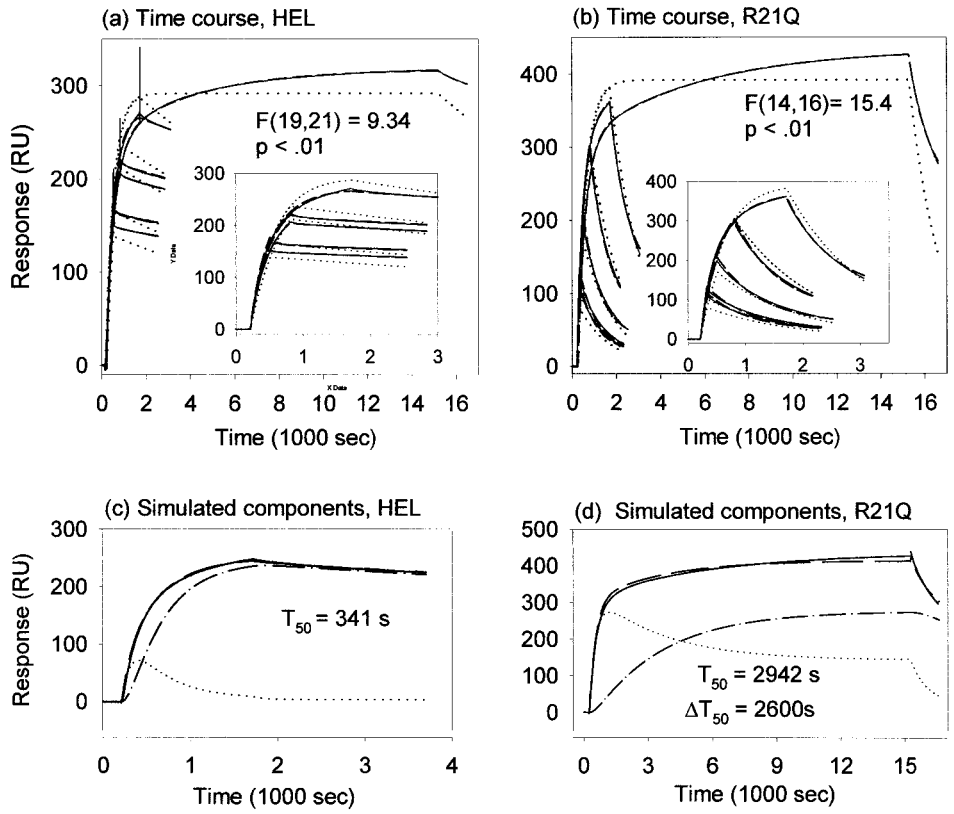

FIGURE 2: Two-step binding by H10. (a, b) Sensogram overlays of a representative time series of rFab10 binding to immobilized (a) 187RU HEL and (b) 291RU HEL(R21Q) (b, d). The parameters in Table 1 were calculated from "*N*" sets of time series data for each respective antibody−antigen complex. In each case, the solid lines (—) represent observed data, dotted lines (•••) represent a global fit to a 1:1 Langmuir model, and dashed lines (- - -) represent a global fit to a two-step association model. Insets show detail of first 45 min of time series. The *F* values represent the ratios of mean squares residuals of the 1:1 fit as the numerator and the two-step fit as denominator, with degrees of freedom defined as the number of data curves minus the number of parameters. **, $p < 0.01$; *, $p < 0.05$. In a typical experiment, each set of curves would be analyzed globally to get single estimates of the rate constants which then would be averaged with other experiments. Table 1 gives the numbers of data sets (*N*) used for calculations for each complex. (c, d) Binding curve components of rfFab10 on (c) HEL with $T_a = 25$ min with and (d) HEL(R21Q) $T_a = 250$ min. Total binding to raw data (—) was fit to the two-state model (- - -) to obtain estimates of the four rate constants (Table 1), which were used to simulate the binding curves for the encounter complex [AB]* (•••) and docked complex AB (-•-).

essential to determine whether the second, slower phase of the BIAcore association curves truly represented an inherent step in complex formation rather than an artifact attributable to a nonspecific binding step such as aggregation of Fab or interaction with the matrix. We examined the association profile of purified rFab26 on HEL using a BIAcore-X that had been modified to allow continuous recirculation of the Fab solution over the sensor surface (*34*). This allowed extension of T_a to longer periods than is possible with the BIAcore1000 and 2000 models, due to the fluid handling capacity of the instruments. A specific binding step would be expected to eventually saturate the surface or come to a concentration-dependent equilibrium, while nonspecific binding would not. The results demonstrated that the antibody binding level eventually approached equilibrium after approximately 26−28 h; subsequent addition of higher concentrations of circulating antibody showed that the binding level was approaching saturation at about ~325RUs, a level of binding compatible with the amount of HEL that had been immobilized on the surface (Figure 5). These results are consistent with a slow second phase of specific binding as described by the two-step model.

(*f*) *Direct Calculation of Off Rates from Distinct Phases of Dissociation Curves.* One should be able to directly calculate the off rates from separate phases of the dissociation curve in a truly biphasic interaction. Intervals from the early (first 2 min) and late (last 10 min) portions of 15 binding curves from an H26−HEL(R21Q) time-course experiment were analyzed separately for their off rates. Average off rates of 1.80×10^{-2} and 1.81×10^{-4} were obtained, which are comparable to the values of 1.62×10^{-2} and 1.76×10^{-4} obtained by global analysis for k_{-1} and k_{-2} (Table 1).

(*g*) *Direct Calculation of Apparent Association from Distinct Phases of Association Curves: Only k_{obs} of the First Phase is Concentration Dependent.* The induced fit mechanism was considered to be a subset or special case of a combined induced-fit/conformational isomerism mechanism (*35*−*37*):

$$\begin{array}{ccc} & \overset{k_{+1}}{\underset{k_{-1}}{\rightleftharpoons}} & \\ A + B & & [AB]^* \\ k_i \downarrow \uparrow k_{-i} & & k_{+2} \downarrow \uparrow k_{-2} \\ & \overset{k_{ii}}{\underset{k_{-ii}}{\rightleftharpoons}} & \\ A + B^* & & AB \end{array} \qquad (4)$$

In our experiments, we would not be able to detect the interconversion of analyte isomers (e.g., B and B* as

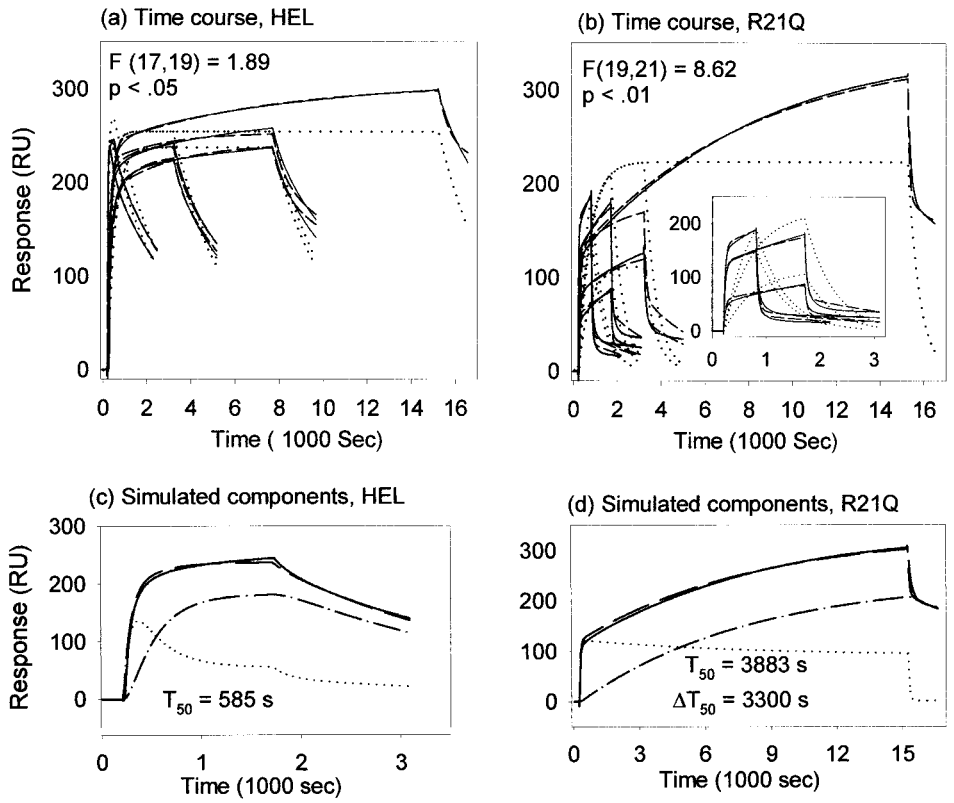

FIGURE 3: Two-step binding by H26. (a, b) Sensogram overlays of representative time series of rFab26 binding to immoblized (a) 187RU HEL and (b) 291RU HEL(R21Q) (b, d, f). Conditions and calculations are as described for Figure 2. (c, d) Binding curve components of rFab26 on (c) HEL with $T_a = 25$ min and (d) HEL(R21Q) $T_a = 250$ min. Components are indicated as in Figure 2.

analyte). The BIAcore binding curves presented here are pre-steady-state kinetics, and during the association phase the analyte concentration is held constant, such that if the antibody were undergoing conformational isomerism the ratios of the conformers are held constant. This would conform to a heterogeneous analyte model in the BIAcore software; fits of our time course data to that model did not result in improved fits, and in many cases the fits were so poor that the calculations aborted due to data overflow (data not shown).

It is possible that there is conformational isomerism within the ligand, however. If B and B* were ligand, eq 4 would predict at least triphasic kinetics. Only biphasic kinetics are apparent in the data presented here, and fitting of the data to a triphasic model consistently yielded poor fits. To distinguish between models represented by eqs 1 and 4, we examined the effect of analyte concentration on the k_{obs} of the two phases. In contrast, in the conformational isomerism model eq 4, both observed rates k_{1obs} and k_{iiobs} of parallel or competitive associations would be dependent on analyte concentration, while k_{+2obs} of docking would be time dependent but not concentration dependent. To distinguish between these two mechanisms, the observed association rates were calculated by regression analysis of the linear portion of the beginning (1−5 min) of the first phase and the last 2−3 min of the second phase of association. These phases can be distinguished for complexes of H26 with both HEL and HEL(R21Q) (Figure 3, panels c and d). The data for the H26−HEL complex are shown in Figure 6, where k_{1obs} is clearly correlated with antibody concentration over nearly 2 orders of magnitude, but k_{+2obs} is largely concentration independent for the second phase. In addition, k_{+2obs} shows more variability than k_{1obs}; inspection of the individual data points shows the variability is related to T_a. The results for the H26−HEL(R21Q) and H10−HEL(R21Q) complexes are similar (data not shown). These results support our interpretation that the two distinct phases in the binding curves detected in our experiments represent stepwise phases (eq 1).

(*h*) *Summary.* We conclude from these experiments that the observed complex kinetics reflect inherent multiphasic Fab−Ag associations and are not a result of artifacts. The data are most consistent with a time-dependent, two-step mechanism rather than parallel or competing associations involving conformational isomers. We also conclude that our preparations of Fab10 and Fab26, whether in unfractionated *E. coli* supernatant, purified, chemically prepared from native antibody, or purified from refolded H and L chains, can be used interchangeably to study the binding kinetics of these Fabs on native and mutant antigen.

Association with HEL. Fab10 associates rapidly with HEL to form the encounter complex [AB]* followed by a slower transition to and accumulation of the more stable AB (Figure 2, panel a). At nanomolar concentrations, the biological half-life of the encounter complex, T_{50}, is ∼5−6 min (Table 1). For this complex, $k_{+2} > k_{-1} > k_{-2}$ (Figure 7, panel a), indicating a faster rearrangement than dissociation of either the encounter or docked complex so the complex will approach 100% AB (*24*). Under nonsaturating conditions, k_{+1} is rate limiting. Under saturating conditions (e.g., excess analyte), k_{+2} becomes rate limiting, and the value of T_{50} reaches a minimum, $T_{50(MIN)} = T_{1/2}$ of k_{+2} (Table 1) (*24*).

In contrast, in the Fab26−HEL complex $k_{+2} \approx k_{-1} > k_{-2}$, and thus there is a closer balance of encounter and docking

Table 1: Summary of Kinetic Parameters for Wild Type Abs

	Fab10		Fab26	
	HEL	R21Q	HEL	R21Q
N^a	14(68)	5(19)	15(61)	4(26)
rate constants[b]				
k_1 ($10^5\,M^{-1}\,s^{-1}$)	1.72	0.98	0.96	0.15
k_{-1} ($10^{-4}\,s^{-1}$)	12.5	13.6	29.3	162
k_2 ($10^{-4}\,s^{-1}$)	40.4	5.9	27	3.6
k_{-2} ($10^{-4}\,s^{-1}$)	1.34	4.09	7.23	1.76
$T_{1/2}$, k_{-1} (s)	554	510	237	43
$T_{1/2}$, k_2 (s)	172	1174	257	1925
T_{50} (s)[c]				
T_{50}, 10 nM	341	2942 (1601)	585	3883 (3298)
(ΔT_{50}, mut-wt)				
$T_{50(MIN)}$	172	1881 (1709)	291	2550 (2259)
($\Delta T_{50(MIN)}$, mut-wt)				
rate determining step	k_1	k_2	k_1/k_2	k_2
equilibrium constants[d]				
K_A ($10^8\,M^{-1}$)	43.9	1.72	1.50	0.029
Ka_1 ($10^7\,M^{-1}$)	13.8	7.22	3.17	0.11
Ka_2	30.2	1.38	3.74	2.03
free energy changes				
(kcal/mol)				
$\Delta G°$	−13.0	−10.9 (2.1)	−11.0	−8.7 (2.3)
($\Delta\Delta G°$, mut-wt)				
$\Delta G1$	−11.0	−10.7 (0.3)	−10.1	−8.1 (2.0)
($\Delta\Delta G1$, mut-wt)				
$\Delta G2$	−2.0	−0.2 (1.8)	−0.9	−0.6 (0.3)
($\Delta\Delta G2$, mut-wt)				
apparent on/off rates[e]				
k on ($10^5\,M\,s^{-1}$)	2.3	1.0	1.7	0.09
k off ($10^{-4}\,s^{-1}$)	0.5	8.4	4.9	60.9

[a] N, number of independent data sets used to determine rate constants, each set consisting of 3−10 sensograms representing a set of purified intact antibody (Ig) or recombinant Fab on a single surface with variable T_a. The total number of sensograms for the wild-type complexes exceeded the maximum allowable number of parameters in the BIAeval3.0.2 software, so data sets were grouped by sensor chip surface, each group containing T_a of at least two different durations. Typical data sets are shown in Figure 2, panels a and b, and Figure 3, panels a and b. Data within each group were analyzed globally to obtain estimates of rate constants. The rate constants from independently determined groups of sensograms were natural log transformed and used to calculate means for each parameter. Error terms on the transformed means and all other parameters were derived from the distributions of the transformed means by Monte Carlo simulation using the function "Gaussian" in the program SigmaPlot (Jandel Scientific) and were all less than 5% of the means. Calculations were performed carrying three significant figures. Total number of sensograms in all data sets combined are shown in parentheses. [b] The parameters k_{+1}, k_{-1}, k_{+2}, k_{-2}, and R_{max} were estimated with BIAeval 3.0.2 software (Biacore, Inc., Uppsala, Sweden) which uses the Marquat−Levenberg algorithm to simultaneously iteratively fit binding data of all curves within a given data set (global fit) to simultaneous rate equations:

$$dB/dt = k_{+1}\cdot A\cdot B - k_{-1}[AB]^*$$

$$d[AB]^*/dt - (k_{+1}\cdot A\cdot B - Tk_{-1}\cdot[AB]^*) - (k_{+2}\cdot[AB]^* - k_{-2}\cdot AB)$$

$$dAB/dt = k_{+2}\cdot[AB] - k_{-2}\cdot AB$$

where $B(0) = R_{max}$, $[AB]^*(0) = AB = 0$, and total $RU = [AB]^* + AB$. [c] Values for T_{50}, determined from simulations using the rate constants determined by global analysis (*24*). All values are given in seconds. [d] Equilibrium constants were calculated from the mean rate constants (*24*) $Ka_1 = k_1/k_{-1}$; $Ka_2 = k_2/k_{-2}$; and $K_A = Ka_1\,(1 + Ka_2)$. [e] From ref *14*.

steps (Figure 7, panel c) such that k_{+2} is likely partially rate limiting. The transition step $[AB]^* \rightarrow AB$ is relatively slower. Given sufficient time, the complex can approach an equilibrium that is ≤ 100%AB, because $k_{+2} > k_{-2}$, indicating relatively stable final complex. At nanomolar concentrations T_{50} 0.10 min, while under saturating conditions, docking becomes rate limiting as in the Fab10−HEL complex, but

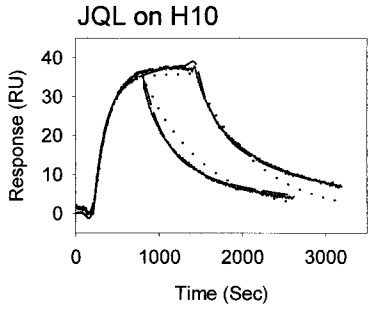

FIGURE 4: JQL binding to sulfhydryl-coupled HyHEL-10 exhibits two-step kinetics. Total binding to raw data (—) was fit to the two-state model (- - -) and simple 1:1 Langmuir model (···).

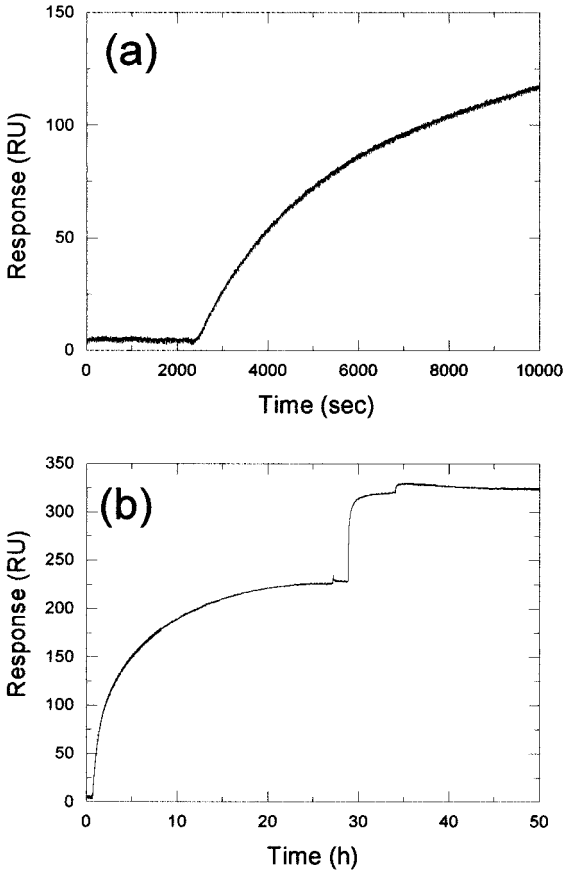

FIGURE 5: Long-term binding kinetics of H26. Long-term association profile of purified rFab26 on immobilized HEL (155RU) in a BIA-x modified to allow continuous recirculation of analyte (*34*); at time zero, 4 μL of 100 nM rFab26 was added; after ∼28 h, 4 μL of 10 μM rFab26 was added; at ∼36 h an additional 16 μL of 10 μM rFab26. The initial binding profile (a) is similar to that seen at the lower concentrations in the BIAcore (Figure 2, panel e). The long-term binding profile (b) shows that equilibrium is initially approached after ∼26 h; the subsequent additions of higher concentrations show that the binding is approaching saturation, as there is only a small increase in RUs bound at the highest concentration. With 155 RUs of HEL immobilized, the expected R_{max} would be between 230 and 465 RUs (assuming 50 and 100%, respectively, of immobilized molecules had the epitope accessible).

$T_{50(MIN)} > T2$ of k_{+2} (*24*). Thus, Ka_1, Ka_2, and overall K_A, are lower than for Fab10. Under saturating conditions, this complex would reach an equilibrium at AB < 100% (*24*).

In summary, in their complexes with HEL, the forward rate constants of Fab10 are higher than those of Fab26, and k_1 is rate limiting, whereas k_2 may also be partially rate limiting for Fab26. The dissociation rate constant k_{-1} of

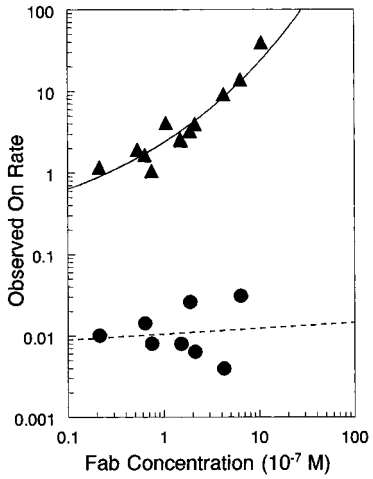

FIGURE 6: Observed association rates of the two association phases of the Fab26−HEL complex. Observed association rates were calculated by linear regression to the first (▲—▲) and last (●- - -●) 1−3 min of Fab26−HEL binding curves.

[Fab−HEL]* encounter complex of Fab10 is lower than that of [Fab26-HEL]*. The dissociation rate constant k_{-2} for Fab−HEL is higher for Fab26 than for Fab10. The docking equilibrium as well as the overall equilibrium constants for Fab26 are lower than those for Fab10.

Mutations of $R21_{HEL}$ Change Rate-Limiting Steps in H10 and H26 Complexes. (*a*) *Association with HEL(R21Q).* The mutation HEL(R21Q) alters the rate-limiting step in both complexes, such that with the mutant antigen $k_{+2} < k_{-1} \geq k_{-2}$ and at all concentrations docking is rate limiting (Figure 7). At physiological concentrations, $T_{50} \sim 1$ h (Table 1; Figures 2d and 3d). Both complexes will come to equilibrium because $k_{+2} \geq k_{-2}$, but at significantly less than 100% AB.

The Fab10−HEL(R21Q) complex differs from the Fab10−HEL complex where k_{-1} is rate limiting (Figure 7, panels a and b). The change in the relative values of k_{-1} and k_2 is attributable to a significant decrease in k_2 as compared to the Fab10−HEL complex. As a consequence, the equilibrium constant for docking, $K\mathrm{a}_2$, of the Fab10−HEL(R21Q) complex is only a third that of the Fab10−HEL complex. The higher apparent net off rate in the mutant complex is attributable to slower docking, rather than to large increases in the dissociation rate constants, because at any point in time there is a higher proportion of less stable encounter complex present (Figure 2, panels c and d). Thus, in association with H10 the HEL(R21Q) mutation changes the rds from encounter to docking.

The equilibrium constant for encounter, $K\mathrm{a}_1$, of Fab10 with HEL(R21Q) is 2−3-fold lower than with HEL, attributable to a slight decrease of k_1 (Table 1, Figure 7, panel b). In contrast, the net $K\mathrm{a}_1$ of Fab26 with HEL(R21Q) is approximately 50-fold lower than with HEL, attributable to a nearly 10-fold lower k_{+1} and a 5-fold higher k_{-1} (Table 1, Figure 7, panels c and d). Thus, the apparent lower net on rate of Fab26 on HEL(R21Q) (*14*) reflects both a lower k_{+1} and a higher k_{-1}.

A similar shift toward docking rate being limiting is seen in the Fab26−HEL(R21Q) complex, but the changes in the underlying rate constants are more complex (Figure 7, panels c and d). Both k_{+2} and k_{-2} are lower and $K\mathrm{a}_2$ is only slightly lower for Fab26−HEL(R21Q) than for Fab26−HEL. However, because $k_{-1} \gg k_{+2}$, it takes a long time for the complex to come to equilibrium except at very high concentrations, and even after 4 h a significant proportion is in the unstable, encounter form (Figure 3, panel d). Thus, an initial rapid net dissociation, reflecting primarily k_{-1}, is observed, followed by a slow dissociation phase (Figure 3). The apparently higher net off rate is attributable solely to dissociation of the encounter complex, as can be seen by comparing the $k_{\mathrm{off(app)}}$ with k_{-1} and k_{-2} (Table 1).

In summary, in the complex with HEL(R21Q) the net encounter equilibrium ($K\mathrm{a}_1$) of Fab26 is lower than that of Fab10. The encounter off rates, k_{-1}, are similar for both Fab on HEL, but show a 10-fold variation on HEL(R21Q), accounting for the 10-fold variation in apparent net k_{on} as analyzed by a one-step model (*14*). In the complex Fab10 with HEL(R21Q), $K\mathrm{a}_1$ falls slightly (3-fold or less), while that of Fab26 falls by over 10-fold. Thus, the apparently more variable on rate of Fab26 reflects variation in both the on and off rate constants of the initial encounter step (k_{+1} and k_{-1}). The apparently higher off rates of Fab10 observed in the one-step analysis of its complex with HEL(R21Q) (*14*) reflects primarily a slower docking (a longer T_{50}), while in the Fab26−R21Q complex it reflects both slower docking (and longer T_{50}) and faster dissociation of the encounter complex. Overall, in the process of complex formation with lysozyme, the mutation $\mathrm{R21}_{\mathrm{HEL}}\mathrm{Q}$ affects primarily the docking phase of Fab10 association, and both the encounter and the docking phase of Fab26. Over a range of concentrations the Fab10−HEL complex is a fast binder, Fab26−HEL is somewhat slower, and Fab10−HEL(R21Q) and Fab26−HEL(R21Q) are the slowest binders.

(*b*) *Complexes with other $R21_{HEL}$ variants.* We examined binding to HEL(R21A) and HEL(R21H) as well as to JQL which contains the natural variation $\mathrm{R21}_{\mathrm{HEL}}\mathrm{Q}$ as well as several other amino acid differences from HEL within the H10 epitope (*14*). Figure 7 compares the rate and equilibrium constants of Fab10 and Fab26 binding to the four variant lysozymes. In the complexes of H10 with both HEL(R21A) and HEL(R21H), the patterns are qualitatively similar to that in the H10−HEL(R21Q) complex (Figure 7, panels a and b). Both of the encounter rate constants change only slightly if at all, and there is a shift in the rate-limiting step toward the docking step due to decreases in k_2. The net equilibrium constants fall by approximately 4-, 10-, and 25-fold, respectively, in the HEL(R21H), HEL(R21A), and HEL(R21Q) complexes with H10 (Figure 7, panel b). In contrast, the encounter equilibria fall by less than 2 for H10−HEL(R21Q) and H10−HEL(R21H), and actually increases slightly for H10−HEL(R21A). Thus, the decreases in overall affinity for all three of these complexes are primarily attributable to decreases in the docking equilibrium constants. The rate-limiting step in the H10−JQL complex also shifts to the docking step, but the underlying dynamics are entirely different. Again, k_1 changes insignificantly, but the other three rate constants, including k_2, all increase and $k_{-1} > k_2 \geq k_{-2}$. In this complex, both dissociation rate constants k_{-1} and k_{-2} increase more than does k_2, hence both $K\mathrm{a}_1$ and $K\mathrm{a}_2$ fall (Figure 7, panels a and b).

The effects of the $\mathrm{R21}_{\mathrm{HEL}}\mathrm{A}$ and $\mathrm{R21}_{\mathrm{HEL}}\mathrm{H}$ mutations on the kinetics of H26−HEL association are very similar to those of $\mathrm{R21}_{\mathrm{HEL}}\mathrm{Q}$: In all complexes of H26 with HEL(R21X), k_{+1} is decreased and k_{-1} is increased, and both of the docking rate constants decrease relative to the complex

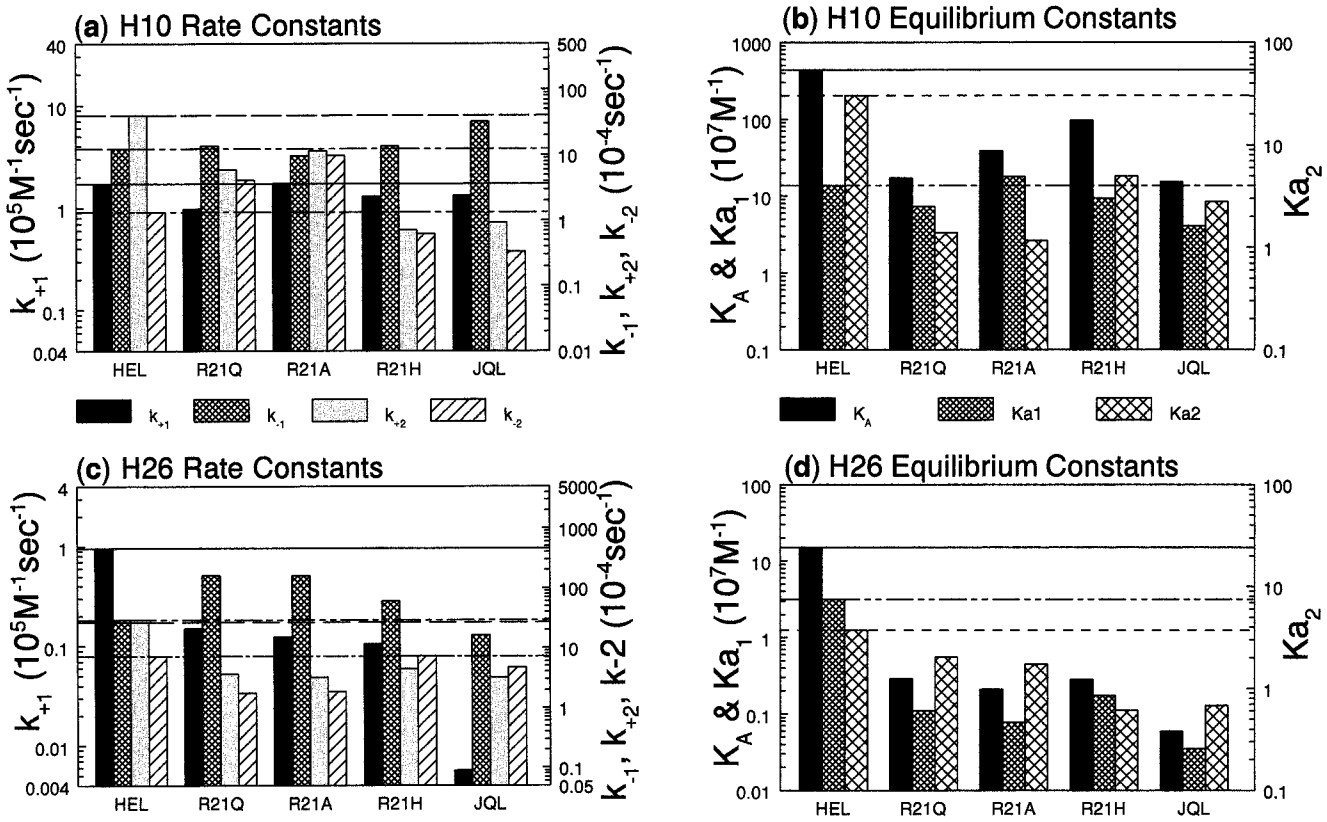

FIGURE 7: Effect of $R21_{HEL}$ mutants on rate and equilibrium constants of complexes with H10 and H26.

with HEL (Figure 7, panel c). In all, both the docking and encounter equilibrium constants are depressed, and docking is rate limiting but the docked complex is relatively stable because $k_{-1} > k_2 > k_{-2}$ (Figure 7, panel d). A similar pattern is seen in the equilibrium constants of the Fab26−JQL complex, but like the H10−JQL complex the underlying dynamics are slightly different. The decrease in the encounter equilibrium is entirely attributable to an increase in k_{-2}, while both of the docking rate constants increase. However, the relationship $k_{-1} > k_2 > k_{-2}$ also holds for this complex, producing net changes in the equilibria and free energy that are similar to those of the site-directed mutants.

In summary, in H10−HEL(R21X) and H26−HEL(R21X) complexes, the rate-limiting step is shifted to docking, in contrast to the wild-type H10−HEL H26−HEL complexes where the rate-limiting step is encounter. The reduction in affinity is due to lower k_2 rate constants producing lower docking equilibria. The impact of the three different residue substitutions on stability of the docked complex varies, but it is clear that the primary energy barrier in $R21_{HEL}X$ mutants is the docking step. The sequence variations in JQL, which include R21Q, also cause slowed docking but in addition low encounter rates. The underlying dynamics include increases in k_{-2} and in both docking rate constants.

Free Energy Changes. For the complexes of both antibodies with wild type and mutant antigen, the majority of free energy change accompanies the encounter step (Figure 8, panels a and c). In the H10 complexes, with the three site-directed mutants, decreases in $\Delta G°$ were nearly entirely associated with the docking step (Figure 8, panel b). In contrast, in the H10−JQL complex free energy change is lost from both steps (Figure 8, panel b), reflecting the decreases in both Ka_1 and Ka_2 in this complex. The free energy change loss associated with the docking step (1.9 kcal/mol) was equivalent to that in HEL(R21Q) and R21A, with the remainder (1.2 kcal/mol) lost from the encounter step. Thus, there is an increased energy barrier to both steps in JQL.

The Fab26−HEL complex gains less than 0.5 kcal/mol from docking, accounting for most of the affinity difference from the Fab10−HEL complex (Figure 8, panel c). Most of the free energy change loss associated with lower affinity is lost from the encounter phase of all three H26−HEL(R21X) complexes and the H26−JQL complex (Figure 8, panel d).

DISCUSSION

Evidence for a Two-Step Binding Mechanism. The association of the structurally and functionally related mAbs H26 and H10 with native and mutant HEL can be described by a two-step bimolecular association model (Figure 1, eq 1) which we interpret to correspond to a fast encounter (or collision) followed by a slower docking (or annealing) (*11*). We chose this model because a large body of accumulating experimental and computational data in our laboratory suggested possible differences in conformational flexibility among the antibodies. The model allows estimation of two forward rate constants (k_{+1}, k_{+2}) and two reverse rate constants (k_{-1}, k_{-2}). The rate constants k_{+2} and k_{-2} are not true off and on rates, but rather are rates of monomolecular complex conversion between the undocked and the docked form. They modulate the observed off and on rates when they become rate limiting, i.e., when $k_{+2} < k_{+1}$, or $k_{-2} < k_{-1}$, and therefore are frequently detectable as distinct phases in the binding and dissociation profiles. Although the three phases may be apparent, robust estimates of both sets of rate constants require simultaneous fitting by global analysis of

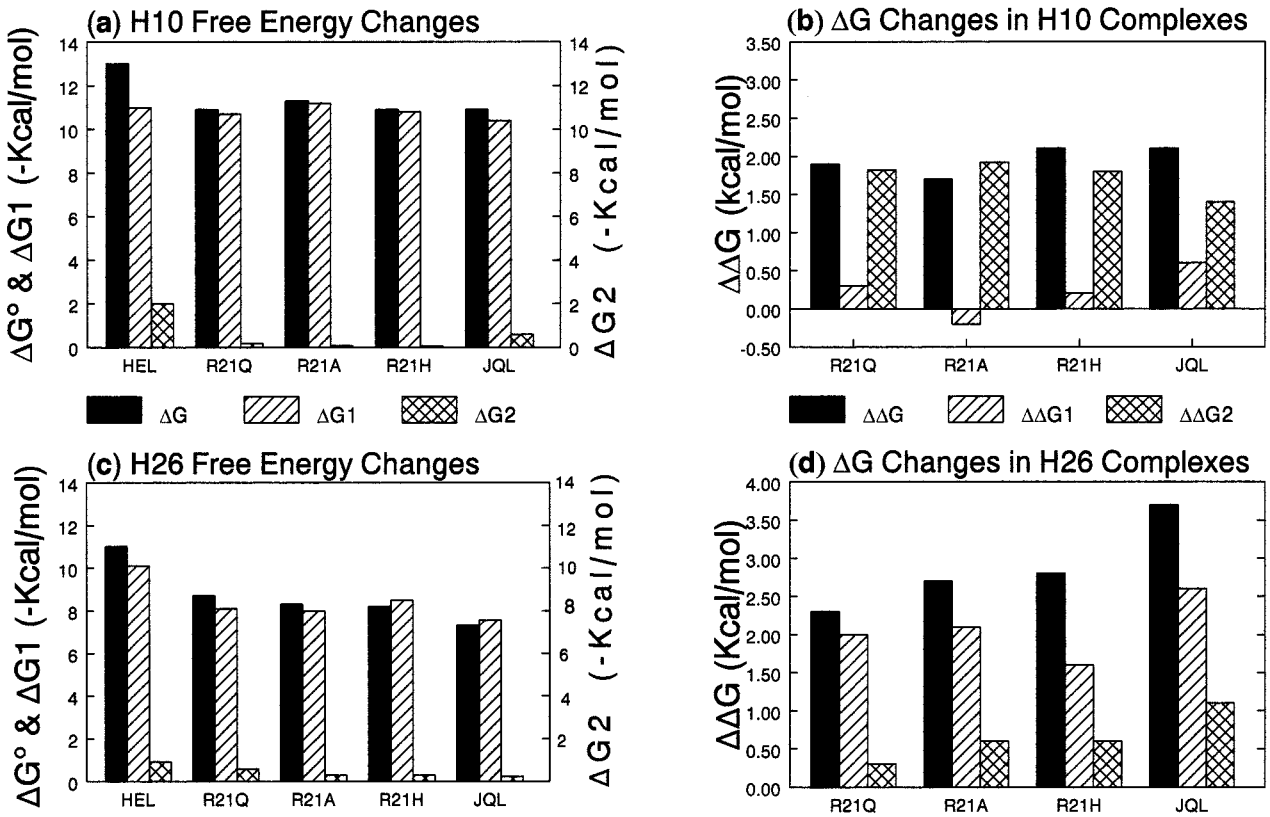

FIGURE 8: Free energy changes in complexes of H10 and H26 with $R21_{HEL}$ mutants. Values of $\Delta\Delta G$ are calculated as $\Delta G_{mut} - \Delta G_{wild\ type}$.

a series of binding curves, because both steps are occurring simultaneously and docking is dependent on the encounter step. In the complexes of both Abs with native HEL, the encounter step is rate limiting, while mutations of $R21_{HEL}$ shift the rate-limiting step to the docking phase.

We have presented here and elsewhere (*24*) controls and experiments that demonstrate that the observed complex kinetics are not attributable to experimental factors such as impurities and/or heterogeneity of the antibodies or the ligand, nonspecific binding, antibody aggregation, and/or coupling-induced ligand heterogeneity. Two-step kinetics are independent of whether antibody or antigen are used as soluble analyte. In addition to statistical analyses of the binding curves, which are necessary but not sufficient to prove a binding mechanism, two sets of data derived from the kinetics provide evidence for a two-step, time-dependent mode of bimolecular association. First, the observed net off rate is inversely correlated with the T_a, an expected result with time-dependent accumulation of a stable, docked complex (*32*, *38*). The quantitative relationship between T_a and net apparent dissociation rate is distinct and characteristic of each antibody−antigen complex, and varies with mutations of either HEL or the antibodies. In addition, direct estimates of k_{obs} from the two distinct phases of association have shown that for the first step k_{obs} is strongly correlated with analyte concentration, while k_{obs} of the second detectable phase is not correlated with concentration but does show variation with T_a. This observation favors an induced-fit model (eq 1) over a competitive or parallel conformational isomerism association process (eq 4). This would not preclude a combined conformational isomerism/induced fit mechanism but does suggest that the two steps we can detect in the current experiments conform most closely to a two-step model (eq 1). The induced fit could involve antibody and/or antigen.

Dynamics of H10 and H26 Association with Lysozyme. The kinetics of complex formation with HEL by the H26 and H10 wild type Fabs are similar, with an initial rapid formation of an encounter complex that rapidly makes the transition to the docked phase, as can be seen by the crossing of the simulated transition and encounter curves (Figures 1−3). The biological half-life (T_{50}) of the H10 encounter complex is ∼5 min, while that of H26 is somewhat longer (∼10 min half-life). The two wild type complexes are probably similarly biologically active despite 10-fold variations in their K_A. The rate constants k_1 are rate limiting in their associations with HEL (*39*), and thus encounter is the rate-determining step (rds) (*40*). The values of k_1 for both Fabs with HEL (Table 1) are equivalent to those found for the net k_a in single step analysis (Table 1) (*14*).

Bi- or triphasic binding kinetics was first described for anti-hapten antibodies (*35*, *37*, *41*, *42*), but have not previously been described for antibody−protein associations. The observation that anti-DNP myeloma proteins exhibit biphasic or triphasic kinetics is particularly relevant, as the antibody MOPC460 expresses V_H36−60 and Vκ23 genes and thus is structurally related to the anti-HEL antibodies described here (*43*, *44*). In fact, the heavy chain sequence of MOPC460 corresponds to the V_H36−60 germ line gene utilized by both H10 and H26 heavy chains (*14*). Thus, there is precedence in the literature for V_H36−60 and Vκ23 antibodies showing multistep binding likely including (but not necessarily limited to) induced fit, supporting our interpretation of the kinetics observed in the current study. Furthermore, a fourth V_H36−60/Vκ23 antibody, H63 whose epitope is also coincident with that of H10, has recently been

shown by X-ray crystallography to undergo small concerted conformational changes in V_H CDR3 upon HEL binding (*1*).

The dynamics of the native complexes are consistent with those described recently for a set of catalytic Abs, namely, a multiphase "induced fit" mechanism consisting of a rapid bimolecular association followed by a slower unimolecular isomerization (*11*). The T_{50}'s observed for the wild-type complexes here (5−10 min) are comparable in magnitude to the $t_{1/2}$ measured for the isomerization step of catalytic antibody−ligand complexes (*11*), and they may be typical of many antibody associations with complex antigens. Although 5−10 min may seem slow, it is important to remember that this interval reflects a shifting population ratio, not the interval required for any given complex to dock. The components analyses in fact show that stable complexes accumulate rapidly (Figures 2c and 3c).

Mutations of residue $R21_{HEL}$ slow docking by both antibodies and dramatically change the dynamics of the complexes with both Ab. They each eventually form stable docked complexes with HEL(R21Q), but only a very small proportion of bound Fab10 or Fab26 makes a transition during the time course of a typical experiment with T_a of 25 min (Figures 2d and 3d). For both Fab−HEL(R21Q) complexes, $k_{-2} \leq k_{+2} \leq k_{-1}$, indicating the encounter complexes dissociate faster than they rearrange, and therefore k_{+2} is the rate-limiting forward constant. The simulated components of the overall kinetics suggest that in complex with HEL(R21Q), Fab10 and Fab26 both undergo significant rearrangement only with experimental $T_a \geq 125$ min. At saturation, these complexes reach an equilibrium with significantly less than 100% AB (*24*). The $R21_{HEL}Q$ mutation also has a detrimental effect on formation of the encounter complex with Fab26. The net lower on rate reflects a 5−6-fold lower k_{+1} and higher k_{-1}. Thus, the net slower association in the H26−HEL(R21Q) complex is attributable to a slower formation of encounter complex coupled with a slower net entry of that complex into the docked phase. In contrast, in the H10−HEL(R21Q) complex slower net association reflects only a slower docking phase. The lower encounter rate of H26 with the mutant antigen may reflect a greater sensitivity to the charge change of the $R21_{HEL}Q$ mutation, consistent with the observation that the H26 combining site is more polar and has a greater number of charged residues (S. Mohan, N. Sinha, and S. Smith-Gill, unpublished).

Although HEL(R21X) mutations cause increases in the net off rates in H10 complexes, the underlying dynamics for all the mutants examined is a lowering of the forward docking rate, rather than greatly increased dissociation rates. Kelley and colleagues (*45*) have observed that stabilization of a protein−protein complex requires docking and that defects in the docking process could manifest as increased apparent dissociation rates. Our results with HEL(R21X) support that view. For example, in association with H10, the effect of the $R21_{HEL}Q$ mutation is seen as an apparently higher net off rate (*14*) (Table 1), but in fact k_{-1} and k_{-2} are each only slighter higher than in the wild type complex. However, because docking is about an order of magnitude slower, some relatively unstable encounter complex is always detectable, i.e., the mutation slows docking and shifts the equilibrium toward [AB]*. In contrast, docking occurs so rapidly in the wild type complex that dissociating encounter complex is not significantly detectable, even with T_a as short as 2 min. Taylor et al. (*23*) argued that the rds in the environment of $R21_{HEL}$ was formation of the encounter complex, and that the transition state for docking of H10 is early in the environment of residue $R21_{HEL}$. Our results indicate that only the docking step is altered by the $R21_{HEL}X$ mutations in H10 complexes. The lowered affinity of H10 for mutant antigen is associated with a significant slowing of docking and a loss of most of $\Delta G2$. Our results are consistent with the interpretation that H10 is able to undergo favorable rearrangement only with wild-type residue at $R21_{HEL}$.

In contrast, an insignificant free energy change accompanies docking of H26, even with native HEL. The lowered affinity of H26 complexes with mutant antigen is accompanied primarily by a significant loss of $\Delta G1$. H26 either docks without rearrangement, or alternatively, undergoes a somewhat slower rearrangement with an unfavorable energetic cost that offsets the formation of an energetically stable docked complex. Preliminary results with other site-directed mutants of HEL are consistent with this conclusion. In aggregate, our results suggest that the free energy barriers to conformational rearrangement are higher in H26 than in H10, particularly when associating with a mutated antigen. This explains the low values of $\Delta G2$ and the extremely long T_a needed to bring Fab26 to equilibrium with HEL (Table 2, Figure 5).

Several other antibodies when undergoing an induced fit to mutant or related antigens or to anti-idiotypic antibodies manifest significantly lowered net association rates. These lower rates have been interpreted to reflect energetically unfavorable conformational changes necessary to achieve complementarity (*46*, *47*). Our analysis is consistent with such an interpretation. Favorable docking rearrangements appear to correlate with favorable $\Delta G2$ changes. Induced fit, cross-reactivity, and also flexibility may correlate with $\Delta G2$. Small $\Delta G2$ as well as large $\Delta\Delta G2$ in association with mutant antigen may indicate a low ability to undergo induced fit.

Parameters of Two-Step Bimolecular Association. As mentioned previously, when multiphasic antibody binding kinetics were initially described for myeloma proteins binding low-affinity hapten ligands, induced fit was considered a special case of a combined mechanism (eq 4) (*35*, *37*, *44*). Although at least triphasic kinetics would be predicted by this model, only biphasic kinetics have generally been observed by others with only a few exceptions (*16*). It has also been suggested (*35*) that even a simple induced fit would actually involve at least three steps:

$$A + B \overset{1a}{\rightleftharpoons} [AB]^\circ \overset{1b}{\rightleftharpoons} [AB]^* \overset{2}{\rightleftharpoons} AB \qquad (5)$$

In this scheme, step 1a would represent formation of a labile transition state complex ([AB]°), while step 1b would correspond to hydrogen-bond exchange and/or fast conformational rearrangement of contact residues of both ligand and analyte to form an encounter complex ([AB]*). Steps 1a and 1b might not be resolvable but together result in a single fast step. This is likely the case for the kinetics of H26 and H10 complexes, interpreted according to this model, because although biphasic curves are readily apparent for complexes of both antibodies with many different site-

directed mutants, we have not observed apparent triphasic kinetics. Step *2* would include larger monomolecular (conformational) rearrangement of proteins in the complex involving higher energetic barriers, and therefore would be a distinct slow step, as we have observed for H10 and H26. The conformational rearrangement undoubtedly also has a labile transition state which in the present experiments is not resolvable.

The two-step analysis (eq 1) allows calculation of T_{50}, which describes the biological half-life of the encounter complex. The parameters T_{50} and T_{50}(MIN) may be better indicators of relative biological activity than the net K_A of a complex. An antibody with rapid docking would be more biologically active than one with slow docking, even if the final docked complexes were equally stable. For example, the net K_A of the H26−HEL complex is 10-fold lower, equivalent to that of H10−HEL(R21Q), but due to its relatively low T_{50} it is likely to be much more biologically active than its affinity would suggest. Similarly, although the affinity of H10−HEL(R21Q) is over 100 times higher than that of H26−HEL(R21Q), both complexes would probably be biologically ineffective because they require 45 min to 1 h to accumulate significant amounts of stable complex, even though both are tight once they form.

Implications for Antibody Repertoire and Affinity Maturation. Affinity maturation is likely to produce antibodies in which the on rate is maximally selected and becomes diffusion limited (*48*). This would maximize Ka_1. As shown above, when $k_2 \leq k_{-1}$, docking is the rds and would naturally be subject to selection. It follows that affinity maturation would also select for fast docking, i.e., short T_{50}, which would require selection for $k_2 > k_{-1}$, thus also maximizing Ka_2. Affinity maturation might also select for more favorable $\Delta G2$. This is consistent with short T_{50}'s observed in the two wild-type complexes described here, and with the observation that the net association rates of most high affinity antibodies are diffusion limited (*50*).

It has been suggested that affinity maturation increases affinity by stabilizing a "preconfigured binding site" through a network of intramolecular polar interactions (*49*); we suggest that this would apply primarily to the initial encounter complex. The impact of such selection would be to increase the net on rate (*9*, *16*, *48*) and to maximize the free energy change of the encounter complex ($\Delta G1$). On the other hand, affinity selection may further modify the combining site to lower the energy barrier to conformational rearrangements, thereby facilitating a docking involving an induced fit and further stabilizing the complex. Although only a few additional kcal of free energy may be derived from the second step ($\Delta G2$), this can represent several orders of magnitude difference in affinity. Therefore, in primary response antibodies the docking step would be rate limiting, with a shift toward the encounter step becoming rate limiting as affinity maturation proceeds. H26 is a somewhat lower affinity binder than H10, and its binding may correspond more to a "lock-and-key" mechanism: it derives very little free energy from docking, which is slower than that of H10. In addition, the initial encounter rates of H26 are somewhat lower and less robust. It is notable that H26 was obtained earlier in the time course of the immune response (*50*) and its sequence is closer to that of the germ line gene than that of H10 (*14*), and therefore may represent a somewhat earlier stage of affinity maturation than H10. Thus, the "lock-and-key" and "induced fit" modes of binding do not necessarily represent a dichotomy of binding modes but rather may delineate sequential steps in the overall association process.

ACKNOWLEDGMENT

We are grateful to Peter Schuck for help with the BIA-X experiments and helpful suggestions on the manuscript. We thank Neeti Sinha for suggestions on the manuscript, and Susan Sharrow for the use of the BIAcore2000 instrument.

SUPPORTING INFORMATION AVAILABLE

Description of cloning of antibody genes and construction of expression vectors, table of primer sequences (Table S1), diagram of construct (Figure S1), sensogram overlays of concentration series with single T_a of 25 min (Figure S2), binding profiles of fractions of rFab (Figure S3), mixing of rFab10 and IgG H10 (Figure S4), and relationship of apparent off rate to T_a of rFab10 and rFab26 on HEL and HEL(R21Q) (Figure S5). This material is available free of charge via the Internet at http://pubs.acs.org.

REFERENCES

1. Li, Y., Li, H., Smith-Gill, S. J., and Mariuzza, R. A. (2000) *Biochemistry 39*, 6296−6309.
2. Ross, P. D., and Subramanian, S. (1981) *Biochemistry 20*, 3096−3102.
3. Padlan, E. A. (1994) *Mol. Immunol. 31*, 169−217.
4. Padlan, E. A. (1994) *Antibody−Antigen Complexes*, R. G. Landes Co., Austin, TX.
5. Alzari, P. M., Lascombe, M. B., and Poljak, R. J. (1988) *Annu. Rev. Immunol. 6*, 555−580.
6. Bhat, T. N., Bentley, G. A., Fischmann, T. O., Boulot, G., and Poljak, R. J. (1990) *Nature 347*, 483−485.
7. Braden, B. C., Dall'Acqua, W., Eisenstein, E., Fields, B. A., Goldbaum, F. A., Malchiodi, E. L., Mariuzza, R. A., Schwarz, F. P., Ysern, X., and Poljak, R. J. (1995) *Pharm. Acta Helv. 69*, 225−230.
8. Conte, L. L., Chothia, C., and Janin, J. (1999) *J. Mol. Biol. 285*, 2177−2198.
9. Foote, J., and Milstein, C. (1991) *Nature 352*, 530−532.
10. Patten, P. A., Gray, N. S., Yang, P. L., Marks, C. B., Wedemayer, G. J., Boniface, J. J., Stevens, R. C., and Schultz, P. G. (1996) *Science 271*, 1086−1091.
11. Lindner, A. B., Eshhar, Z., and Tawfik, D. S. (1999) *J. Mol. Biol. 285*, 421−430.
12. Smith-Gill, S. J., Lavoie, T. B., and Mainhart, C. R. (1984) *J. Immunol. 133*, 384−393.
13. Newman, M. A., Mainhart, C. R., Mallett, C. P., Lavoie, T. B., and Smith-Gill, S. J. (1992) *J. Immunol. 149*, 3260−3272.
14. Lavoie, T. B., Mohan, S., Lipschultz, C. A., Grivel, J. C., Li, Y., Mainhart, C. R., Kam-Morgan, L. N., Drohan, W. N., and Smith-Gill, S. J. (1999) *Mol. Immunol. 36*, 1189−1205.
15. Lavoie, T. B., Drohan, W. N., and Smith-Gill, S. J. (1992) *J. Immunol. 148*, 503−513.
16. Foote, J., and Milstein, C. (1994) *Proc. Natl. Acad. Sci. U.S.A. 91*, 10370−10374.
17. Padlan, E. A., Silverton, E. W., Sheriff, S., Cohen, G. H., Smith-Gill, S. J., and Davies, D. R. (1989) *Proc. Natl. Acad. Sci. U.S.A. 86*, 5938−5942.
18. Kondo, H., Shiroishi, M., Matsushima, M., Tsumoto, K., and Kumagai, I. (1999) *J. Biol. Chem. 274*, 27623−27631.
19. Novotny, J. (1999) *Mol. Immunol. 28*, 201−207.
20. Kam-Morgan, L. N., Smith-Gill, S. J., Taylor, M. G., Zhang, L., Wilson, A. C., and Kirsch, J. F. (1993) *Proc. Natl. Acad. Sci. U.S.A. 90*, 3958−3962.
21. Pons, J., Rajpal, A., and Kirsch, J. F. (1999) *Protein Sci. 8*, 958−968.

22. Rajpal, A., Taylor, M. G., and Kirsch, J. F. (1998) *Protein Sci. 7*, 1868−1874.
23. Taylor, M. G., Rajpal, A., and Kirsch, J. F. (1998) *Protein Sci. 7*, 1857−1867.
24. Lipschultz, C. A., Li, Y., and Smith-Gill, S. (2000) *Methods* 310−318.
25. Krauss, G., Riesner, D., and Maass, G. (1976) *Eur. J. Biochem. 68*, 81−93.
26. Riesner, D., Pingoud, A., Boehme, D., Peters, F., and Maass, G. (1976) *Eur. J. Biochem. 68*, 71−80.
27. Morton, T. A., Myszka, D. G., and Chaiken, I. M. (1995) *Anal. Biochem. 227*, 176−185.
28. Rousseau, P. G., Mallett, C. P., and Smith-Gill, S. J. (1989) *Mol. Immunol. 26*, 993−1006.
29. Lavoie, T. B., Kam-Morgan, L. N. W., Hartman, A. B., Mallett, C. P., Sheriff, S., Saroff, D. A., Mainhart, C. R., Hamel, P. A., Kirsch, J. F., Wilson, A. C., and Smith-Gill, S. J. (1989) in *The Immune Response to Structurally Defined Proteins: The Lysozyme Model* (Smith-Gill, S., and Sercarz, E., Eds.) pp 151−167, Adenine Press, Syracuse, NY.
30. Barre, S., Greenberg, A. S., Flajnik, M. F., and Chothia, C. (1994) *Nat. Struct. Biol. 1*, 915−920.
31. Schuck, P. (1997) *Curr. Opin. Biotechnol. 8*, 498−502.
32. Karlsson, R., and Falt, A. (1997) *J. Immunol. Methods 200*, 121−133.
33. Lavoie, T. B., Kam-Morgan, L. N. W., Mallett, C. P., Schilling, J. W., Prager, E. M., Wilson, A. C., and Smith-Gill, S. J. (1990) in *The Use of X-ray Crystallography in the Design of Anti-Viral Agents* (Laver, G. W. and Air, G. M., eds) pp 213−232, Academic Press, New York.
34. Schuck, P. (1998) *Anal. Biochem. 265*, 79−91.
35. Haselkorn, D., Friedman, S., Givol, D., and Pecht, I. (1974) *Biochemistry 13*, 2210−2222.
36. Zidovetzki, R., Licht, A., and Pecht, I. (1981) *Mol. Immunol. 18*, 491−497.
37. Pecht, I., and Lancet, D. (1977) *Mol. Biol. Biochem. Biophys. 24*, 306−338.
38. Malmqvist, M., and Karlsson, R. (1997) *Curr. Opin. Chem. Biol. 1*, 378−383.
39. Wallis, R., Leung, K. Y., Pommer, A. J., Videler, H., Moore, G. R., James, R., and Kleanthous, C. (1995) *Biochemistry 34*, 13751−13759.
40. Schreiber, G., and Fersht, A. R. (1993) *Biochemistry 32*, 5145−5150.
41. Vuk-Pavlovic, S., Blatt, Y., Glaudemans, C. P., Lancet, D., and Pecht, I. (1978) *Biophys. J. 24*, 161−174.
42. Lancet, D., Licht, A., Schechter, I., and Pecht, I. (1977) *Nature 269*, 827−829.
43. Lancet, D., and Pecht, I. (1976) *Proc. Natl. Acad. Sci. U.S.A. 73*, 3549−3553.
44. Zidovetzki, R., Blatt, Y., and Pecht, I. (1981) *Biochemistry 20*, 5011−5018.
45. Kelley, R. F., Costas, K. E., O'Connell, M. P., and Lazarus, R. A. (1995) *Biochemistry 34*, 10383−10392.
46. Braden, B. C., Fields, B. A., Ysern, X., Goldbaum, F. A., Dall'Acqua, W., Schwarz, F. P., Poljak, R. J., and Mariuzza, R. A. (1996) *J. Mol. Biol. 257*, 889−894.
47. Leder, L., Berger, C., Bornhauser, S., Wendt, H., Ackermann, F., Jelesarov, I., and Bosshard, H. R. (1995) *Biochemistry 34*, 16509−16518.
48. Foote, J., and Eisen, H. N. (1995) *Proc. Natl. Acad. Sci. U.S.A. 92*, 1254−1256.
49. Wedemayer, G. J., Patten, P. A., Wang, L. H., Schultz, P. G., and Stevens, R. C. (1997) *Science 276*, 1665−1669.
50. Mallett, C. P., Rousseau, P. G., Saroff, D. A., and Smith-Gill, S. J. (1989) in *The Immune Response to Structurally Defined Proteins: The Lysozyme Model* (Smith-Gill, S. J., and Sercarz, E. E., Eds.) pp 353−368, Adenine Press, New York.

BI0014148